Journal of Applied Physics

Martensitic transformations of β-phase in zirconium

Cite as: J. Appl. Phys. **129**, 225103 (2021); https://doi.org/10.1063/5.0053723
Submitted: 10 April 2021 . Accepted: 21 May 2021 . Published Online: 09 June 2021

Appala Naidu Gandi, and Jiajie Zhu

View Online Export Citation CrossMark

ARTICLES YOU MAY BE INTERESTED IN

Deformation of binary and boron-doped Ni_3Al alloys at high pressures studied with synchrotron x-ray diffraction
Journal of Applied Physics **129**, 225101 (2021); https://doi.org/10.1063/5.0037012

Optical phonon modes, static and high-frequency dielectric constants, and effective electron mass parameter in cubic In_2O_3
Journal of Applied Physics **129**, 225102 (2021); https://doi.org/10.1063/5.0052848

Controllable probe absorption spectrum via vortex beams excitation in a cascaded atomic system
Journal of Applied Physics **129**, 224303 (2021); https://doi.org/10.1063/5.0050488

© 2021 Author(s).

Journal of Applied Physics ARTICLE scitation.org/journal/jap

Martensitic transformations of β-phase in zirconium

Cite as: J. Appl. Phys. **129**, 225103 (2021); doi: 10.1063/5.0053723
Submitted: 10 April 2021 · Accepted: 21 May 2021 ·
Published Online: 9 June 2021

View Online Export Citation CrossMark

Appala Naidu Gandi[1,a)] and Jiajie Zhu[2]

AFFILIATIONS

[1]Department of Metallurgical and Materials Engineering, Indian Institute of Technology Jodhpur, Jodhpur 342037, India
[2]College of Materials Science and Engineering, Shenzhen University, Nanhai Ave. 3688, ShenZhen, Guangdong 518060, People's Republic of China

[a)]**Author to whom correspondence should be addressed:** appalanaidu@iitj.ac.in

ABSTRACT

Martensitic transformations in the body-centered cubic β-phase ($Im\bar{3}m$) of zirconium are studied using first-principles calculations, group-theoretical methods, and symmetry analysis. Phonon dispersion relations in the β-phase calculated within the harmonic approximation predicted an unstable phonon at wave vector $\frac{2\pi}{a}\left[\frac{1}{2}, \frac{1}{2}, 0\right]$(N) and a soft phonon at wave vector $\frac{2\pi}{a}\left[\frac{2}{3}, \frac{2}{3}, \frac{2}{3}\right]$($\Lambda$). The symmetry of the unstable phonon is the same as the symmetry of the N_4^- irreducible representation, and the symmetry of the soft phonon is the same as the symmetry of the Λ_1 irreducible representation. Martensitic transformations are simulated considering two steps. Frozen phonon calculations are used to determine the first step, i.e., the transformation of the β-phase to an intermediate phase due to phonon motion. Structure relaxation is used to determine the second step, i.e., the transformation of the intermediate phase to the final phase. The unstable N_4^- phonon transforms the β-phase into an intermediate orthorhombic phase (Cmcm), which further transforms to a hexagonal close packed α-phase ($P6_3/mmc$) after structure relaxation. The soft Λ_1 phonon transforms the β-phase into an intermediate trigonal phase ($P\bar{3}m1$), which further transforms to a hexagonal close packed ω-phase (P6/mmm) after structure relaxation. The intermediate phase space group ($Cmcm/P\bar{3}m1$) is a common subgroup of the parent phase (β) space group and the final phase (α/ω) space group. Therefore, the martensitic transformations in zirconium are reconstructive transformations of the second kind. Symmetry characterization of the martensitic transformations is also presented.

Published under an exclusive license by AIP Publishing. https://doi.org/10.1063/5.0053723

I. INTRODUCTION

Zirconium (Zr) has good strength, high ductility, good fabricability, and good corrosion resistance for a wide range of chemical media, along with the low absorption cross section for neutrons.[1] Due to these properties, Zr is primarily used as a cladding material in nuclear reactors and chemical process industries. Zr crystallizes into a body-centered cubic β-phase ($Im\bar{3}m$) on solidification.[2] The β-phase is stable up to 862 °C and undergoes a martensitic transformation into a hexagonal α-phase ($P6_3/mmc$) on further cooling.[3] The α-phase is stable up to room temperature under ambient pressure conditions. Relative stability of phases is also affected by pressure. A compressive pressure of 2.2 GPa transforms the α-phase into the ω-phase (P6/mmm) at ambient temperatures.[4] On further increase in pressure above 30 ± 2 GPa, the ω-phase transforms into the β-phase.[4] On removal of pressure, the reverse β–ω–α transformation is observed. Properties of a material depend on the constituent phases in the microstructure. Understanding different characteristics of the martensitic transformations helps us in designing better materials.

The β–ω transformation happens through a longitudinal phonon motion of wave vector $\frac{2\pi}{a}\left[\frac{2}{3}, \frac{2}{3}, \frac{2}{3}\right]$.[5,6] The phonon polarization is such that one of the (222) planes of the β phase is immobile while two adjacent successive planes move toward each other. The symmetry of the distorted structure is a trigonal symmetry during the transformation, and the transformation is complete when the two neighboring (222) planes moving in opposite directions joined together and results in a P6/mmm symmetry.[7–9]

Earlier, the Burgers mechanism explained the structural changes that happen during the β–α transition in terms of shear on (112) planes of the β phase.[10] Later on, phonon softening was observed experimentally at two wave vectors: $\frac{2\pi}{a}\left[\frac{1}{2}, \frac{1}{2}, 0\right]$ and $\frac{2\pi}{a}\left[\frac{2}{3}, \frac{2}{3}, \frac{2}{3}\right]$.[11] The atomic motion of the soft phonon at the $\frac{2\pi}{a}\left[\frac{1}{2}, \frac{1}{2}, 0\right]$ wave vector is along the $[1\bar{1}0]$ direction, and, hence, it is a transverse acoustic (TA) phonon motion.[12] The Burgers

Published under an exclusive license by AIP Publishing

mechanism is further refined, and the β–α transition is explained in terms of the TA phonon motion.[13] The atoms move along the [111] direction in the case of the soft phonon at the $\frac{2\pi}{a}\left[\frac{2}{3}, \frac{2}{3}, \frac{2}{3}\right]$ wave vector, and, hence, it is a longitudinal acoustic (LA) phonon motion.[12] The β–ω transition is explained in terms of the LA phonon motion.[14]

Ground state harmonic phonon calculations of the β-phase suggested dynamic instability for a TA phonon motion at the $\frac{2\pi}{a}\left[\frac{1}{2}, \frac{1}{2}, 0\right]$ wave vector and atomic motion of a few phonons along the $\frac{2\pi}{a}[\xi, \xi, \xi]$ direction.[15,16] However, the frozen phonon calculations suggested small activation energy for the LA phonon motion with wave vector $\frac{2\pi}{a}\left[\frac{2}{3}, \frac{2}{3}, \frac{2}{3}\right]$ and the resulting symmetry is shown to be P$\bar{3}$m1 trigonal symmetry.[17] Group-theoretical analysis predicted that a Cmcm orthorhombic structure would form due to the TA phonon instability and a P3m1/P$\bar{3}$m1 trigonal structure would form due to the LA phonon instability.[18] Experimentally, the orthorhombic α'' phase was observed in the quenched Zr–1.5 at. % Re alloy,[19] Zr–Mo alloys (1.5–2.0 at. % Mo), and Zr–Ta alloys (5–11 at. % Ta),[20] and the trigonal (P$\bar{3}$m1) phase was observed in Zr–Nb alloys (8–15 wt. %).[21,22]

The martensitic transformations in Zr happen through the cooperative movement of atoms, and the β-phase transforms to either the α phase or the ω phase through an intermediate phase, and hence these transformations are reconstructive transformations of the second kind.[23] These transformations involve unstable phonon motion as well as lattice deformation. By listing the subgroups of the β and the α phase space groups, Bendersky *et al.* identified an orthorhombic intermediate phase (Cmcm) for the β–α transformation.[24] Recently, we have characterized the martensitic transformation in Ti by considering the following two steps: (a) transformation of the parent β-phase to an intermediate phase due to unstable phonon motion and (b) transformation of the intermediate phase to the final phase (α/ω) due to lattice deformation.[25] The present work employs a similar approach for studying the martensitic transformation in Zr. The first objective of this work is to simulate the martensitic transformations in Zr using frozen phonon calculations and structural optimization methods. The second objective of this work is to characterize the martensitic transformations.

II. METHODOLOGY

Density functional theory based calculations were performed using the Vienna *ab initio* Simulation Package.[26] Potentials constructed by following the all electron projector augmented wave method were used.[27] The exchange-correlation energy is approximated within the generalized gradient approximation using the Perdew–Burke–Ernzerhof functional.[26,28] Twelve valence electrons of Zr (4*s*, 4*p*, 4*d*, and 5*s*) were considered in the calculations of electronic states. The electronic wave functions were expanded using plane waves with kinetic energies up to 300 eV. Issues due to the partial occupation of the electronic states near the Fermi level (due to the metallic nature of Zr) were addressed with the Methfessel–Paxton smearing method.[29] A smearing width of 0.1 eV was used. The α, β, and ω unit cells were optimized using $24 \times 24 \times 16$, $24 \times 24 \times 24$, and $15 \times 15 \times 24$ Γ-centered *k*-meshes, respectively.

An open body-centered cubic structure is stabilized at high temperatures due to large vibrational entropy originating from the phonon–phonon interactions. With the decrease in the temperature, the phonon–phonon interactions reduce and the phonon motion becomes independent at low temperatures. On further cooling, softening of a phonon mode and subsequent transformation of the β-phase occur due to the phonon instability. The phonon dispersion relation calculated within the harmonic approximation represents the independent phonons qualitatively well. A small displacement method was employed to calculate the harmonic phonon dispersion relation by constructing $3 \times 3 \times 2$, $6 \times 6 \times 6$, and $3 \times 3 \times 2$ supercells of α, β, and ω unit cells, respectively.[30,31] $8 \times 8 \times 8$, $4 \times 4 \times 4$, and $9 \times 9 \times 4$ *k*-meshes were used during the Brillouin zone integration while calculating the forces on atoms in the supercells of the α, β, and ω unit cells, respectively. Experimentally observed soft phonon symmetries were determined as per the symmetries of the respective phonon motion in the calculated harmonic phonon dispersion. Using the irreducible representation of the unstable/soft phonons, the symmetry of the product phases (that would form due to the phonon motion) and the order parameters for the corresponding transitions were determined assuming the parent clamping approximation.[32] The transformations of the β were simulated using the frozen phonon calculations, and the lowest energy modulated structures were realized.[33] These lowest energy structures were considered as the intermediate phases.

The minimum energy modulated structures were under remnant pressure (up to 1.5 GPa) as the structures were not allowed to relax. The remnant pressure was relieved by allowing the atoms to relax and the lattice to deform until the forces on each atom reached below 0.01 eV/Å. During the structure optimization of the intermediate phases with Cmcm and P$\bar{3}$m1 symmetries, $24 \times 24 \times 14$ and $15 \times 15 \times 24$ *k*-meshes were used. Lattice deformation, increase in the symmetry, reduction in energy, and transformation of the intermediate Cmcm/P$\bar{3}$m1 phase to the final α/ω phase were observed during the structure optimization. Symmetry analysis of the final relaxed structures was performed with a tolerance value of 0.01 Å.[34] After simulating the $\beta \rightarrow$ Cmcm/P$\bar{3}$m1 $\rightarrow \alpha/\omega$ transformation, further characterization of each step is done.[35–37] The crystal structure of phases that are involved in the martensitic transformation was depicted using the VESTA.[38]

III. RESULTS AND DISCUSSION

Relaxed structural parameters of the β, α, and ω phases presented in Table I are in agreement with the experimental values. Calculated harmonic phonon dispersion relation of the α-phase

TABLE I. Comparison of the relaxed unit cell parameters of the α, β, and ω phases with the experimental values in the literature (values in the parenthesis).

Lattice constants	Zr
β-a (Å)	3.564 (3.579 at 0 K, extrapolated value[39])
α-a (Å)	3.225 (3.229 at 4.2 K[40])
α-c (Å)	5.160 (5.141 at 4.2 K[40])
ω-a (Å)	5.031 (5.036 at 298 K[41])
ω-c (Å)	3.144 (3.109 at 298 K[41])

Published under an exclusive license by AIP Publishing

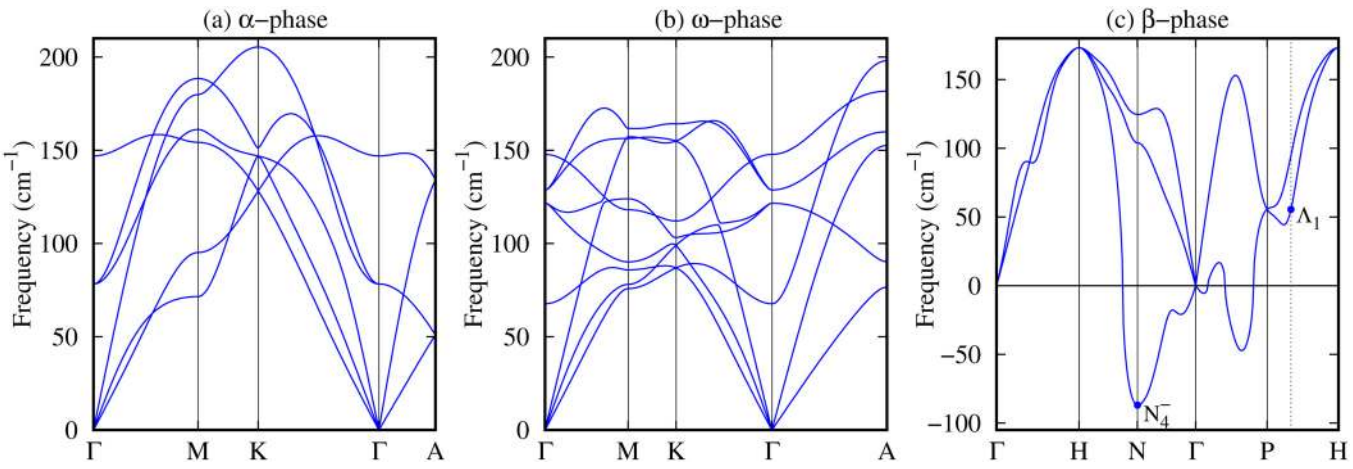

FIG. 1. Calculated phonon dispersion relation in (a) the α-phase, (b) the ω-phase, and (c) the β-phase.

and the ω-phase is shown in Figs. 1(a) and 1(b), respectively. All the frequencies are positive in both these plots, suggesting the dynamic stability of the α-phase and the ω-phase at the ground state. Both these results are in agreement with the previously calculated phonon dispersion relations.[42] In the harmonic phonon dispersion relation for the β-phase [shown in Fig. 1(c)], the imaginary phonon frequencies are plotted as negative values. Here, there is one unstable phonon at the $\frac{2\pi}{a}\left[\frac{1}{2}, \frac{1}{2}, 0\right]$ wavevector (N) and one soft phonon at the $\frac{2\pi}{a}\left[\frac{2}{3}, \frac{2}{3}, \frac{2}{3}\right]$ wavevector (along the Λ path). The unstable phonon polarization at the N-vector is along the $\langle 1\bar{1}0\rangle$ (transverse) direction and it has N_4^- symmetry. The soft phonon polarization at the $\frac{2\pi}{a}\left[\frac{2}{3}, \frac{2}{3}, \frac{2}{3}\right]$ wavevector is along the $\langle 111\rangle$ direction (longitudinal) and it has Λ_1 symmetry. The N_4^- and Λ_1 symmetries are used in the following group-theoretical analysis to determine the unstable/soft phonon induced phase transformations.

A. Dynamic instability of the β-phase

Out of all the possible transformations due to the unstable/soft phonon motion, transformations resulting in phases with either two or three atom unit cells are considered as the experimentally observed low temperature α-phase and ω-phase unit cells have two and three atoms, respectively. Three such transformations are possible, and the data corresponding to the three transformations are presented in Table II. The unstable N_4^- phonon transforms the β-phase into an intermediate phase with Cmcm symmetry. The size of the intermediate Cmcm phase unit cell is twice the size of the β unit cell, and one of the six unstable modes (as can be seen from the order parameter) are active during the transformation. Similarly, the soft Λ_1 phonon can transform the β-phase into two intermediate phases (P3m1 and P$\bar{3}$m1) having three atoms in the unit cell. Two of the eight soft modes are active during the $\beta \rightarrow$ P3m1 transformation, while only one of the eight soft modes is active during the $\beta \rightarrow$ P$\bar{3}$m1 transformation.

TABLE II. Characteristics of martensitic transformations induced due to N_4^- and Λ_1 phonon instability.

Phonon	Space group	Size	Order parameter
N_4^-	Cmcm	2	(0, 0, 0, 0, a, 0)
Λ_1	P3m1	3	(a, b, 0, 0, 0, 0, 0, 0)
Λ_1	P$\bar{3}$m1	3	(a, 0, 0, 0, 0, 0, 0, 0)

To realize the predicted intermediate phases, modulated structures were created using the polarization of unstable/soft phonon. Figure 2 shows the energy variation of the modulated structures with the phonon amplitude. The energy of the modulated structure is decreasing with the amplitude of the unstable N_4^- phonon motion for the $\beta \rightarrow$ Cmcm transformation, reaching a minimum for the largest atomic displacement value of 0.264 Å. Structural relaxation of the minimum energy modulated Cmcm structure further reduced the energy and resulted in the α-structure. The energy of the modulated structure is increasing with the soft phonon Λ_1 amplitude for the $\beta \rightarrow$ P3m1 transformation. In the case of the $\beta \rightarrow$ P-3m1 transformation, the energy is increasing slightly with the soft Λ_1 phonon amplitude, followed by a decreasing trend up to a minimum and an increasing trend with a further increase in the amplitude. The initial energy barrier for the $\beta \rightarrow$ P-3m1 transformation was also observed in previous frozen phonon calculations.[17] The minimum is observed for the largest atomic displacement value of 0.514 Å, which is equal to the $\sqrt{3}a/12$ value required for the formation of a P6/mmm structure.[5,6] Structure optimization of the minimum energy modulated structure reduced the energy further and resulted in the ω-structure. The energy minimization observed during the $\beta \rightarrow$ Cmcm $\rightarrow \alpha$ transformation and the $\beta \rightarrow$ P-3m1 $\rightarrow \omega$ transformation is shown in Fig. 3. The two simulated transformation paths are discussed in more detail in Secs. III B–III D.

Published under an exclusive license by AIP Publishing

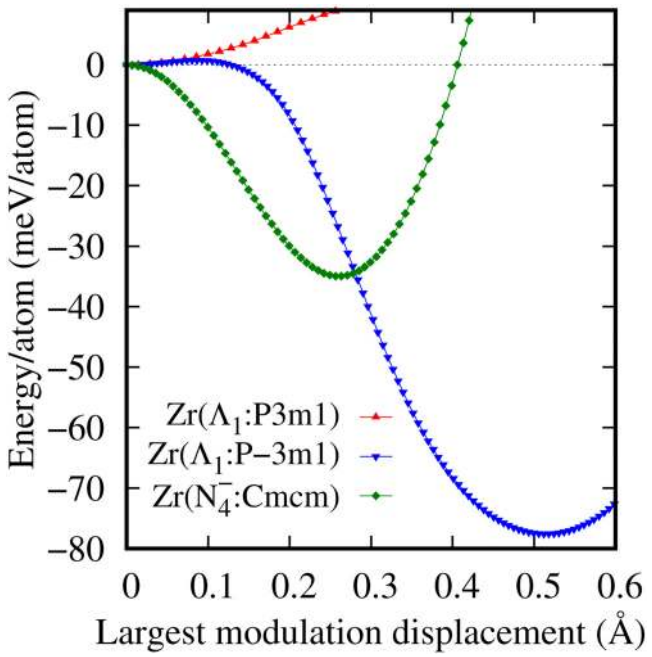

FIG. 2. Energy variation of the modulated structure as a function of the modulation amplitude.

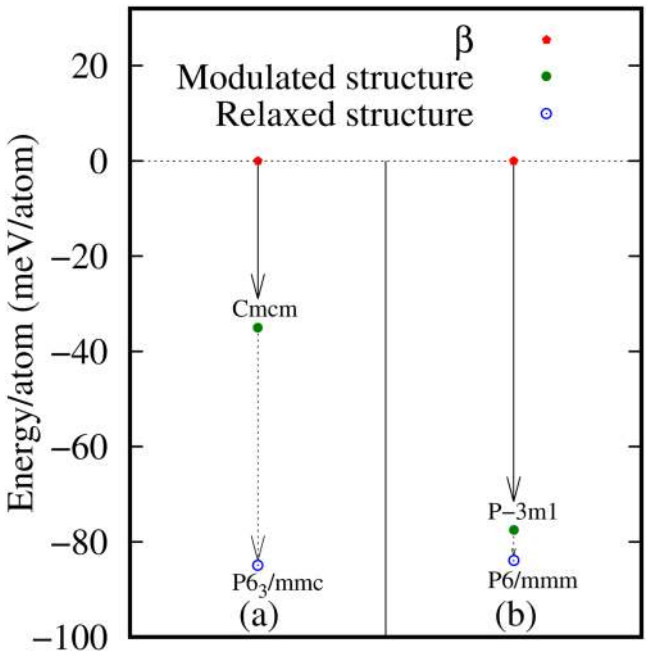

FIG. 3. Energy minimization along two martensitic transformation paths: (a) $\beta \rightarrow$ Cmcm $\rightarrow \alpha$ and (b) $\beta \rightarrow$ P-3m1 $\rightarrow \omega$. In each path, the solid arrow represents the formation of the lowest energy modulated structure from the β-phase and the dotted arrow represents the formation of the α/ω-phase from the lowest energy modulated structure due to structure optimization. Energy values are expressed with respect to the β-phase energy.

B. Im$\bar{3}$m → Cmcm → P6$_3$/mmc

Atomic motion for the formation of the intermediate Cmcm structure is shown as the displacement of the blue atoms to the green atoms in Figs. 4(a)–4(c). Conventional and primitive unit cell axes in the Cmcm structure are marked in orange color and black color, respectively. There are four atoms in the conventional unit cell and two atoms in the primitive unit cell. As can be seen in Fig. 2, the energy decreases for small amplitudes and reaches a minimum when the atomic displacement is equal to 0.264 Å. For this atomic displacement, the conventional cell parameters of the resulting structure are a = 3.564 Å, b = 5.040 Å, and c = 5.040 Å, and the Zr atoms are at 4c Wyckoff positions (y = 0.3023). As shown in Fig. 4(d), there are two atoms in the primitive unit cell and their cell parameters are a = 3.086 Å, b = 3.086 Å, c = 5.04 Å, $\angle\alpha = 90°$, $\angle\beta = 90°$, and $\angle\gamma = 109.47°$. The energy of the system has reduced by 34.96 meV/atom due to the creation of the minimum energy modulated structure. However, a remnant pressure of 1.4 GPa was observed on the created modulated structure. Structure optimization removed the pressure, converted the intermediate Cmcm structure into the α-structure, and reduced the energy by 49.96 meV/atom. Relaxed unit cell [Fig. 4(e)] parameters are within ± 0.001 Å values of the α unit cell parameters, and the Zr atoms are relaxed to the 2c Wyckoff positions. The volume of the unit cell has increased by 2.7%, and the dimensional change during the relaxation can be expressed through the following strain components: $\varepsilon_{xx} = -0.0951$, $\varepsilon_{yy} = 0.1083$, and $\varepsilon_{zz} = 0.0238$. The space group of the resulting α-phase (P6$_3$/mmc) is a super-group of the space group (Cmcm) of the intermediate phase. Therefore, the simulated β-Cmcm-α transformation is validating the predicted reconstructive nature (second kind) of the martensitic transformation in Zr.[24] The orientation relationship between β, Cmcm, and α phases that appear during the simulated martensite transformation is presented in Table III. These results are consistent with the Burgers orientation relationship for the β–α transformation.[10]

C. Im$\bar{3}$m → P$\bar{3}$m1 → P6/mmm

The Λ_1 phonon motion for the formation of the P$\bar{3}$m1 structure is shown in Figs. 5(a)–5(c). In this motion, two adjacent (222) planes move toward each other while the successive (222) plane remains stationary.[5,6] There is a small energy barrier for the smaller phonon amplitudes reflecting the dynamic stability of the β-phase as indicated by the positive phonon frequency (see Fig. 2). However, with a further increase in the phonon amplitude, the energy is reduced and it reached a minimum (−77.55 meV/atom) when the two (222) planes moved by 0.514 Å and joined together. Symmetry of the modulated structure is P$\bar{3}$m1 until the joining of the two moving (222) planes, and it has changed to P6/mmm symmetry (symmetry of the ω-phase) on joining of the two (222) planes.

Figure 5(d) shows the unit cell of the minimum energy modulated structure. Its cell parameters are a = 5.039 Å and c = 3.086 Å,

Published under an exclusive license by AIP Publishing

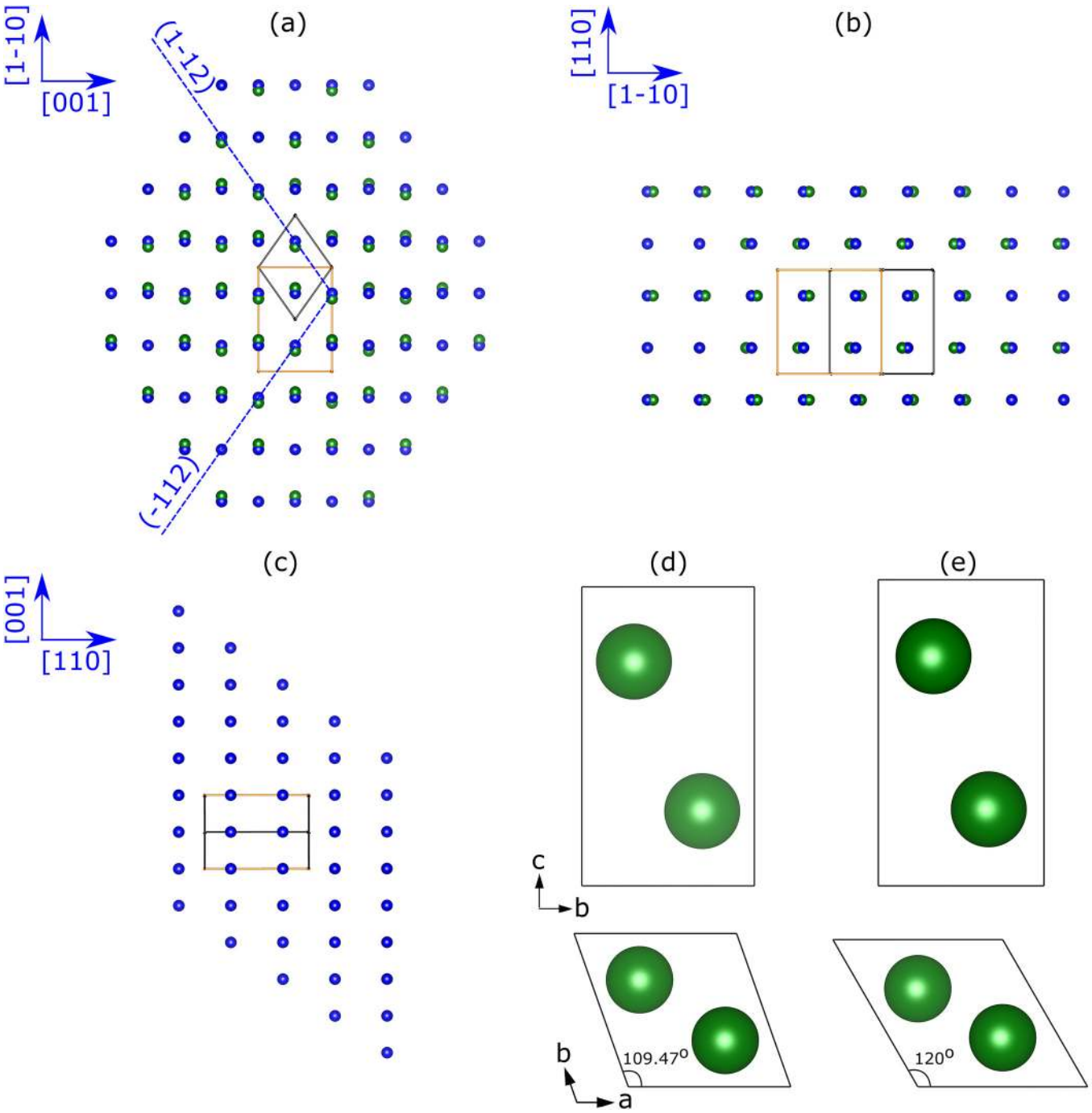

FIG. 4. Creation of a modulated Cmcm orthorhombic structure (green atoms) due to an N_4^- phonon motion at $\frac{2\pi}{a}\left[\frac{1}{2}, \frac{1}{2}, 0\right]$ in the body-centered cubic structure (blue atoms). Conventional and primitive unit cell axes of the modulated structure are highlighted in orange and black colors, respectively. The origin of the conventional unit cell is at $\left(\frac{a_\beta}{2}, 0, 0\right)$ distance from the origin of the β unit cell. (a)–(c) show the projection along the [110], [001], and [1−10] directions of the β-phase, respectively. (d) Primitive unit cell of the minimum energy modulated Cmcm structure and (e) corresponding relaxed unit cell with $P6_3/mmc$ symmetry.

Published under an exclusive license by AIP Publishing

TABLE III. Orientation relationship among various phases observed in the simulated β–Cmcm–α transformation. Atomic planes and directions are indexed with respect to the β and Cmcm conventional unit cells.

Atomic planes
$(001)_\beta \approx (100)_{\mathrm{Cmcm}} \approx (1\bar{1}0) = (1\bar{1}00)_\alpha$
$(1\bar{1}0)_\beta \approx (010)_{\mathrm{Cmcm}} \approx (110) = (11\bar{2}0)_\alpha$
$(110)_\beta \approx (001)_{\mathrm{Cmcm}} \approx (001) = (0001)_\alpha$
Directions
$[1\bar{1}1]_\beta \approx [110]_{\mathrm{Cmcm}} \approx [010] = [\bar{1}2\bar{1}0]_\alpha$
$[\bar{1}11]_\beta \approx [1\bar{1}0]_{\mathrm{Cmcm}} \approx [100] = [2\bar{1}\bar{1}0]_\alpha$
$[110]_\beta \approx [001]_{\mathrm{Cmcm}} \approx [001] = [0001]_\alpha$

TABLE IV. Orientation relationship among various phases observed in the simulated β–P$\bar{3}$m1–ω transformation.

Atomic planes
$(1\bar{1}0)_\beta \approx (100)_{P\bar{3}m1} \approx (100) = (10\bar{1}0)_\omega$
$(\bar{1}01)_\beta \approx (010)_{P\bar{3}m1} \approx (010) = (01\bar{1}0)_\omega$
$(\bar{1}\bar{1}\bar{1})_\beta \approx (001)_{P\bar{3}m1} \approx (001) = (0001)_\omega$
Directions
$[1\bar{1}0]_\beta \approx [100]_{P\bar{3}m1} \approx [100] = [2\bar{1}\bar{1}0]_\omega$
$[\bar{1}01]_\beta \approx [010]_{P\bar{3}m1} \approx [010] = [\bar{1}2\bar{1}0]_\omega$
$[\bar{1}\bar{1}\bar{1}]_\beta \approx [001]_{P\bar{3}m1} \approx [001] = [0001]_\omega$

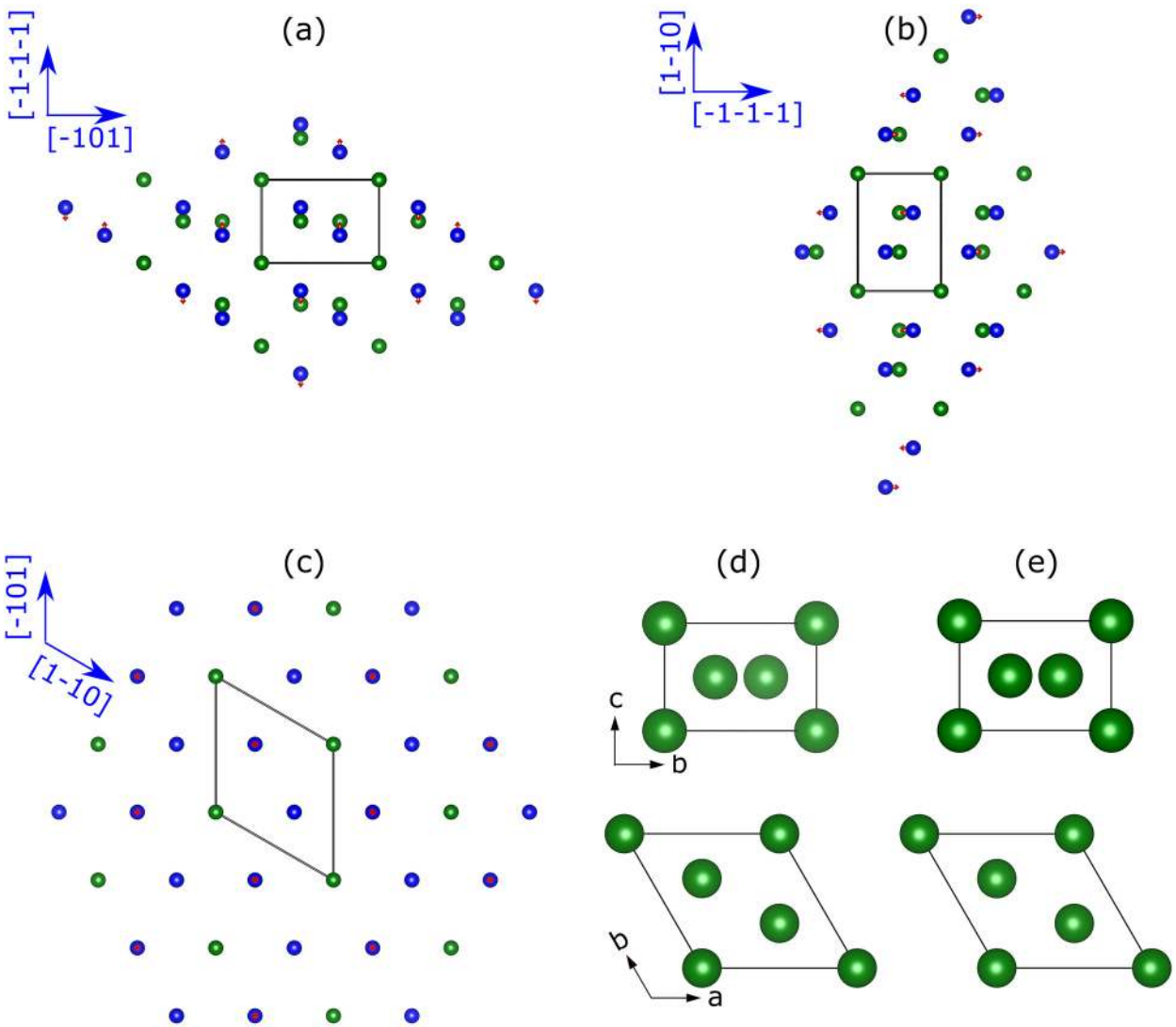

FIG. 5. Creation of a modulated trigonal P$\bar{3}$m1 structure (green atoms) due to a Λ_1 phonon motion (red arrows) at $\frac{2\pi}{a}\left[\frac{2}{3}, \frac{2}{3}, \frac{2}{3}\right]$ in the body-centered cubic structure (blue atoms). (a)–(c) show the projections along the [1−10], [−101], and [−1−1−1] directions of the β-phase, respectively. (d) Unit cell of the lowest energy modulated structure with P6/mmm symmetry and (e) corresponding unit cell after structure optimization.

Published under an exclusive license by AIP Publishing

TABLE V. Symmetry characterization of the transformation of the parent β-phase to the intermediate Cmcm/P$\bar{3}$m1-phase. Here, boldfaced letters denote the unit cell vectors of the parent phase.

Parent phase			Intermediate phase			Index	Transformation matrices
S_1	Z	Wyckoff position	H	Z	Wyckoff position	i	(**P**,**p**)
Im$\bar{3}$m	2	2*a*	Cmcm	4	4*c*	12	$\mathbf{c}+\frac{1}{2}$, $\mathbf{a}+\mathbf{b}$, $-\mathbf{a}+\mathbf{b}$
Im$\bar{3}$m	2	2*a*	P$\bar{3}$m1	3	1*a*,2*d*	12	$-\mathbf{a}+\mathbf{b}$, $-\mathbf{b}+\mathbf{c}$, $\frac{1}{2}\mathbf{a}+\frac{1}{2}\mathbf{b}+\frac{1}{2}\mathbf{c}$

TABLE VI. Symmetry characterization of transformation between the intermediate Cmcm/P$\bar{3}$m1-phase and the product α/ω-phase. Here, boldfaced letters denote the unit cell vectors of the product phase.

Product phase			Intermediate phase			Index	Transformation matrices
S_2	Z	Wyckoff position	H	Z	Wyckoff position	i	(**P**,**p**)
$P6_3/mmc$	2	2*c*	Cmcm	4	4*c*	3	$-\mathbf{a}-\mathbf{b}$, $\mathbf{a}-\mathbf{b}$, **c**
P6/mmm	3	1*a*,2*d*	P$\bar{3}$m1	3	1*a*,2*d*	2	**a**, **b**, **c**

and atoms are at 1*a* and 2*d* Wyckoff positions. Remnant pressure of 1.5 GPa is present on the minimum energy modulated structure. Structure relaxation has removed this pressure. The relaxed unit cell parameters are a = 5.031 Å and c = 3.143 Å, which are in good agreement with the ω unit cell parameters. Figure 5(e) shows the relaxed unit cell. The energy was reduced by 6.43 eV/atom, and the volume was increased by 1.5% during the structure relaxation. The following strain components describe the dimensional changes that occurred during the structure optimization: $\varepsilon_{xx} = -0.0018$, $\varepsilon_{yy} = -0.0018$, and $\varepsilon_{zz} = 0.018\,45$.

Equivalence of planes and the directions in different structures involved in the Im$\bar{3}$m → P$\bar{3}$m1 → P6/mmm transition are shown in Table IV. These relations are consistent with the orientation relationships described in the literature.[7] The intermediate trigonal P$\bar{3}$m1 space group is a subgroup of the ω space group (P6/mmm). Therefore, the simulated path is a reconstructive transformation path.

D. Symmetry characterization

Each simulated transformation path is connecting the parent β-phase to the product α/ω-phase through an intermediate phase and is having two steps. The β-phase transforms into an intermediate phase (Cmcm/P$\bar{3}$m1) during the first step and the intermediate phase transforms into the product phase (α/ω) in the second step. The space group of the intermediate phase (H) is a subgroup of both the space group of the parent β-phase (S_1) and the space group of the product α/ω phase (S_2). There is a one-to-one correspondence between the unit cell of the parent/product phase and the unit cell of the intermediate phase expressed in terms of the following transformation characteristics: space group, number of atoms in the conventional unit cell (Z), Wyckoff positions, index, and transformation matrices relating the conventional unit cells. The transformation characteristics for the first step of the transformation path ($S_1 \leftrightarrow H$) are listed in Table V, and the transformation characteristics for the second step of the transformation path ($H \leftrightarrow S_2$) are listed in Table VI. These results are consistent with the orientation relations and atomic positions presented previously.

Under ambient pressure conditions, the β-phase transforms to the α-phase on cooling in pure Zr.[3] The intermediate orthorhombic phase was observed experimentally in quenched Zr–1.5 at. % Re alloy,[19] Zr–Mo alloys (1.5–2.0 at. % Mo), and Zr–Ta alloys (5–11 at. % Ta).[20] However, so far, no intermediate phase has been reported for pure Zr. This could be due to the faster kinetics of the transformation in pure metals compared to alloys. All these transformation characteristics can be explained using the simulated β–α transformation. Therefore, the martensitic transformation in pure Zr and these Zr-alloys can be understood to be happening due to N_4^- phonon instability. Experimentally, the β–ω transformation is observed in the Zr–Ti alloy (25 at. % Ti)[5] and Zr–Nb alloys (8–15 wt. %).[43] Also, the symmetry of the ω-phase is reported to be trigonal (P$\bar{3}$m1) in Zr–Nb alloys (8–15 wt. %).[21,22] The simulated β–ω transformation in the present study explains all these characteristics. Therefore, the martensitic transformation in these Zr-alloys can be understood to be happening due to the Λ_1 phonon instability. Even though the Λ_1 phonon is calculated to be a soft mode at the ground state in pure Zr, the energy barrier is very low. Experimental observation of the β–ω transformation in certain Zr-alloys suggests that the Λ_1 phonon is softer than that of the N_4^- phonon before the martensitic transformation in these alloys.

IV. CONCLUSIONS

Two martensitic transformations are simulated in Zr using the first-principles calculations and group-theoretical approaches. The transformation of the high temperature β-phase on cooling is explained in terms of its dynamical instability. An unstable N_4^- phonon at the wave vector $\frac{2\pi}{a}\left[\frac{1}{2}, \frac{1}{2}, 0\right]$ is shown to be responsible for the transformation of the β-phase to an orthorhombic Cmcm phase. The intermediate Cmcm phase transforms to the α-phase due to structure relaxation and completes the β–α transformation. A soft Λ_1 phonon at the wave vector $\frac{2\pi}{a}\left[\frac{2}{3}, \frac{2}{3}, \frac{2}{3}\right]$ is shown to be

Published under an exclusive license by AIP Publishing

responsible for the transformation of the β-phase to a trigonal P$\bar{3}$m1 phase. The intermediate trigonal P$\bar{3}$m1 phase transforms to the ω-phase due to structure relaxation and completes the β–ω transformation. Except for a small initial energy barrier for the Λ_1 phonon motion, the overall energy of the system is reducing along each transformation path. The transformation of the intermediate phase (Cmcm/P$\bar{3}$m1) to the product phase (α/ω) can account for the transformation strains associated with the transformation. Symmetry characteristics of the two simulated transition paths are presented, and the transformations are shown to be reconstructive transformations of the second type.

ACKNOWLEDGMENTS

The research presented in this article was supported by the Science and Engineering Research Board through the Early Career Research Award Grant No. ECR/2018/001583/ES. We also thank the Indian Institute of Technology Jodhpur for providing all the facilities.

DATA AVAILABILITY

The data that support the findings of this study are available within the article.

REFERENCES

[1]D. O. Northwood, Mater. Des. **6**, 58–70 (1985).
[2]R. Tricot, J. Nucl. Mater. **189**, 277–288 (1992).
[3]E. S. Fisher and C. J. Renken, Phys. Rev. **135**, A482–A494 (1964).
[4]H. Xia, S. J. Duclos, A. L. Ruoff, and Y. K. Vohra, Phys. Rev. Lett. **64**, 204–207 (1990).
[5]S. L. Sass, Acta Metall. **17**, 813–820 (1969).
[6]D. De Fontaine, Acta Metall. **18**, 275–279 (1970).
[7]S. L. Sass, J. Less Common Met. **28**, 157–173 (1972).
[8]A. Devaraj, S. Nag, R. Srinivasan, R. E. A. Williams, S. Banerjee, R. Banerjee, and H. L. Fraser, Acta Mater. **60**, 596–609 (2012).
[9]D. Banerjee and J. C. Williams, Acta Mater. **61**, 844–879 (2013).
[10]W. G. Burgers, Physica **1**, 561–586 (1934).
[11]A. Heiming, W. Petry, J. Trampenau, M. Alba, C. Herzig, H. R. Schober, and G. Vogl, Phys. Rev. B **43**, 10948–10962 (1991).
[12]W. Petry, A. Heiming, J. Trampenau, M. Alba, C. Herzig, H. R. Schober, and G. Vogl, Phys. Rev. B **43**, 10933–10947 (1991).
[13]Y. Y. Ye, Y. Chen, K. M. Ho, B. N. Harmon, and P. A. Lindgrd, Phys. Rev. Lett. **58**, 1769–1772 (1987).
[14]A. Heiming, W. Petry, J. Trampenau, M. Alba, C. Herzig, and G. Vogl, Phys. Rev. B **40**, 11425–11428 (1989).
[15]P. Souvatzis, O. Eriksson, M. I. Katsnelson, and S. P. Rudin, Comput. Mater. Sci. **44**, 888–894 (2009).
[16]B.-T. Wang, P. Zhang, H.-Y. Liu, W.-D. Li, and P. Zhang, J. Appl. Phys. **109**, 063514 (2011).
[17]K.-M. Ho, C. L. Fu, and B. N. Harmon, Phys. Rev. B **29**, 1575–1587 (1984).
[18]V. P. Dmitriev, S. B. Rochal, Y. M. Gufan, and P. Toledano, Phys. Rev. Lett. **60**, 1958–1961 (1988).
[19]A. V. Dobromyslov and N. I. Taluts, Scr. Mater. **35**, 573–577 (1996).
[20]N. I. Taluts and A. V. Dobromyslov, J. Phys. IV France **112**, 1099–1102 (2003).
[21]W. Lin, H. Spalt, and B. W. Batterman, Phys. Rev. B **13**, 5158–5169 (1976).
[22]S. K. Sikka, Y. K. Vohra, and R. Chidambaram, Prog. Mater. Sci. **27**, 245–310 (1982).
[23]Y. A. Izyumov and V. N. Syromyatnikov, *Phase Transitions and Crystal Symmetry*, Fundamental Theories of Physics (Springer, 1990).
[24]L. A. Bendersky, A. Roytburd, and W. J. Boettinger, Acta Metall. Mater. **42**, 2323–2335 (1994).
[25]A. N. Gandi and J. Zhu, Phys. Status Solidi B **257**, 2000193 (2020).
[26]G. Kresse and D. Joubert, Phys. Rev. B **59**, 1758–1775 (1999).
[27]P. E. Blöchl, Phys. Rev. B **50**, 17953–17979 (1994).
[28]J. P. Perdew, K. Burke, and M. Ernzerhof, Phys. Rev. Lett. **77**, 3865–3868 (1996).
[29]M. Methfessel and A. T. Paxton, Phys. Rev. B **40**, 3616–3621 (1989).
[30]D. Alfè, Comput. Phys. Commun. **180**, 2622–2633 (2009).
[31]A. Togo and I. Tanaka, Scr. Mater. **108**, 1–5 (2015).
[32]H. T. Stokes, S. V. Orden, and B. J. Campbell, J. Appl. Crystallogr. **49**, 1849–1853 (2016).
[33]A. Togo and I. Tanaka, Phys. Rev. B **87**, 184104 (2013).
[34]R. W. Grosse-Kunstleve and P. D. Adams, Acta Crystallogr. A **58**, 60–65 (2002).
[35]C. Capillas, J. M. Perez-Mato, and M. I. Aroyo, J. Phys.: Condens. Matter **19**, 275203 (2007).
[36]E. Kroumova, J. M. Perez-Mato, and M. I. Aroyo, J. Appl. Crystallogr. **31**, 646–646 (1998).
[37]M. I. Aroyo, A. Kirov, C. Capillas, J. M. Perez-Mato, and H. Wondratschek, Acta Crystallogr. A **62**, 115–128 (2006).
[38]K. Momma and F. Izumi, J. Appl. Crystallogr. **44**, 1272–1276 (2011).
[39]A. Heiming, W. Petry, J. Trampenau, W. Miekeley, and J. Cockcroft, J. Phys.: Condens. Matter **4**, 727–733 (1992).
[40]J. Goldak, L. T. Lloyd, and C. S. Barrett, Phys. Rev. **144**, 478–484 (1966).
[41]J. C. Jamieson, Science **140**, 72–73 (1963).
[42]H. Zong, G. Pilania, X. Ding, G. J. Ackland, and T. Lookman, npj Comput. Mater. **4**, 48 (2018).
[43]C. W. Dawson and S. L. Sass, Metall. Mater. Trans. B **1**, 2225–2233 (1970).

Published under an exclusive license by AIP Publishing